HIGH-PRESSURE PHYSICS

Observation of the Wigner-Huntington transition to metallic hydrogen

Ranga P. Dias and Isaac F. Silvera*

Producing metallic hydrogen has been a great challenge in condensed matter physics. Metallic hydrogen may be a room-temperature superconductor and metastable when the pressure is released and could have an important impact on energy and rocketry. We have studied solid molecular hydrogen under pressure at low temperatures. At a pressure of 495 gigapascals, hydrogen becomes metallic, with reflectivity as high as 0.91. We fit the reflectance using a Drude free-electron model to determine the plasma frequency of 32.5 ± 2.1 electron volts at a temperature of 5.5 kelvin, with a corresponding electron carrier density of 7.7 ± 1.1 × 10^{23} particles per cubic centimeter, which is consistent with theoretical estimates of the atomic density. The properties are those of an atomic metal. We have produced the Wigner-Huntington dissociative transition to atomic metallic hydrogen in the laboratory.

Several key problems in physics involving hydrogen include production of the metallic phase, high-temperature superconductivity, and controlled nuclear fusion (*1*). The transition to solid metallic hydrogen (SMH) was envisioned by Wigner and Huntington (WH) more than 80 years ago (*2*). They predicted a first-order dissociative transition to an atomic lattice through compression of solid molecular hydrogen to a sufficiently high density. Solid atomic hydrogen would be a metal with one electron per atom with a half-filled conduction band. Although WH's density for the transition was approximately correct, their predicted pressure of 25 GPa (100 GPa = 1 megabar) was way off because they incorrectly used the zero-pressure compressibility for all pressures. Wigner and Huntington predicted a simple phase diagram. Enormous experimental and theoretical developments dramatically reshaped the phase diagram of hydrogen (Fig. 1) over the past decades. Modern quantum Monte-Carlo methods and density functional theory predict pressures of ~400 to 500 GPa for the transition (*3*–*5*), with an atomic lattice being in the $I4_1/amd$ space group (*5*, *6*). Metallic hydrogen (MH) may be a high-temperature superconductor, predicted by Ashcroft (*7*), with critical temperatures possibly higher than room temperature (*8*, *9*). Moreover, other predictions suggest SMH is metastable at room temperature when the pressure is released (*10*). The combination of these expected properties makes SMH important for solving energy problems and can potentially revolutionize rocketry as a powerful propellant (*11*).

Lyman Laboratory of Physics, Harvard University, Cambridge, MA 02138, USA.
*Corresponding author. Email: silvera@physics.harvard.edu

The pathways to MH require either increasing pressure at low temperature (Fig. 1, pathway I) or increasing temperature to cross the plasma phase transition (Fig. 1, pathway II) (*12*–*17*). Pathway I transitions through a number of phases not envisioned in the simple phase diagram predicted by WH. The low-pressure properties of solid molecular hydrogen are fascinating, and many aspects—such as the importance of ortho-para concentrations, and solid-solid phase transitions characterized by orientational order—have been reviewed elsewhere (*3*, *18*). In the low-pressure, low-temperature phase I, molecules are in spherically symmetric quantum states and form a hexagonal close-packed structure. Phases II, III, and IV are phases with structural changes and orientational order of the molecules (*19*–*23*). A new phase in hydrogen observed at liquid-helium temperatures believed to precede the metallic phase was called H_2-PRE (*24*) [also named VI at higher temperatures (*25*)].

We carried out a rigorous strategy to achieve the higher pressures needed to transform hydrogen to SMH in a diamond anvil cell (DAC). Diamond failure is the principal limitation for achieving the required pressures to observe SMH. We believe that one point of failure of diamonds arises from microscopic surface defects created in the polishing process. We used type IIac conic synthetic diamonds (supplied by Almax-Easylab) with ~30-μm-diameter culet flats. We etched off ~5 μm from the diamond culets using reactive ion etching to remove surface defects (figs. S7 and S8) (*26*). We vacuum annealed the diamonds at high temperature to remove residual stresses. A second point of failure is diamond embrittlement from hydrogen diffusion. Hydrogen can disperse into the confining gasket or the diamonds (at high pressure or temperature). As an activated process, diffusion is suppressed at low temperatures. We maintained the sample at liquid-nitrogen or liquid-helium temperatures during the experimental runs. Alumina is also known to act as a diffusion barrier against hydrogen. We coated the diamonds along with the mounted rhenium (Re) gasket with a 50-nm-thick layer of amorphous alumina through the process of atomic layer deposition. We have found through our extensive experience with alumina coatings at high pressures that it does not affect or contaminate the sample, even at temperatures as high as ~2000 K (*12*). Last, focused laser beams, even at low laser power (10 mW) on samples at high pressures in DACs, can also lead to failure of the highly stressed diamonds. Laser light in the blue spectral region appears to be particularly hazardous because it potentially induces the growth of defects (*27*). Thermal shock to the stressed culet region from inadvertent laser heating is another risk. Moreover, a sufficiently intense laser beam, even at infrared (IR) wavelengths, can graphitize the surface of the diamond. Thus, we studied the sample mainly with very low-power, incoherent IR radiation from a thermal source and minimized illumination of the sample with lasers when the sample was at very high pressures.

We cryogenically loaded the sample chamber at 15 K, which included a ruby grain for pressure determination. We initially determined a pressure of ~88 GPa by means of ruby fluorescence (*26*). Determining the pressure in the megabar regime is more challenging (*26*). We measured the IR vibron absorption peaks of hydrogen at higher pressures (>135 GPa) with a Fourier transform IR spectrometer with a thermal IR source, using the known pressure dependence of the IR vibron peaks for pressure determination (*26*). We did this to a pressure of ~335 GPa, while the sample was still transparent (Fig. 2A). The shift of the laser-excited Raman active phonon of the diamond in the highly stressed culet region is currently the method used for determining pressure at extreme high pressures. For fear of diamond failure due to laser illumination and possible heating of the black sample, we only measured the Raman active phonon at the very highest pressure of the experiment (495 GPa) after the sample transformed to metallic hydrogen and reflectance measurements had been made. We equipped our DACS with strain gauges that allowed us to measure the applied load, which we found was proportional to pressure during calibration runs (*26*). We estimated pressure between 335 and 495 GPa using this calibration. We increased the load (pressure) by rotating a screw with a long stainless-steel tube attached to the DAC in the cryostat. Increasing the pressure by rotating the screw after the 335-GPa pressure point resulted in our sample starting to turn black (Fig. 2B) as it transitioned into the H_2-PRE phase (*24*). Earlier studies of hydrogen reported the sample as black at lower pressures (*28*), but we believe that this is a result of different pressure calibrations in this high-pressure region (*26*).

Erratum 18 August 2017. See Erratum.

After some more screw turns (fig. S3), the sample reflectance changed from black to high reflectivity, characteristic of a metal (Fig. 2C). We then studied the wavelength dependence of the reflectance of the sample at liquid-nitrogen and liquid-helium temperatures (Fig. 3). In order to do this, the stereo microscope, used for visual observation (Fig. 2), was replaced with a high-resolution long-working-distance microscope (Wild Model 420 Macroscope) that not only allowed visual observation but also allowed an attenuated laser beam to be cofocused with the microscope image. In order to measure the reflectance, we wanted to magnify the image of the sample and project it on a camera. The Macroscope (fig. S5) (*26*) enables an external image to be formed that can be further magnified for a total calibrated magnification of ~44; this was imaged onto a color CMOS (complementary metal-oxide semiconductor) camera (DC1645C, Thorlabs). We can select the area of interest (effectively spatial filtering) and measure the reflectance from different surfaces (fig. S6). We measured the reflectance from the MH and the Re gasket. We measured at three wavelengths in the visible spectral region, using both broadband white light and three narrow band lasers that illuminated the sample (*26*), as well as one wavelength in IR. The measured reflectances are shown in Fig. 3, along with measurements of reflectance of the Re gasket and reflectance from a sheet of Re at ambient conditions that agreed well with values from the literature (*29*).

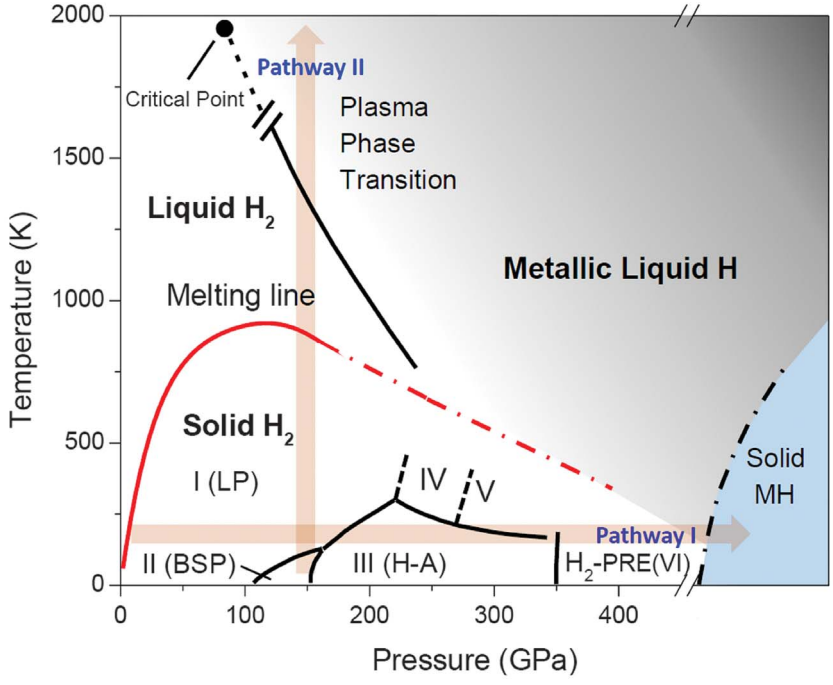

Fig. 1. Experimental/theoretical P-T phase diagram of hydrogen. Shown are two pathways to MH: I is the low-temperature pathway, and II is the high-temperature pathway. In pathway I, phases for pure para hydrogen have lettered names: LP, low pressure; BSP, broken symmetry phase; and H-A, hydrogen-A. The plasma phase transition is the transition to liquid metallic atomic hydrogen.

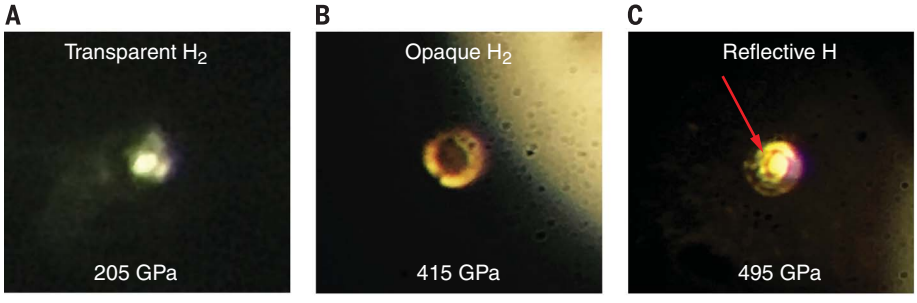

Fig. 2. Photographs of hydrogen at different stages of compression. Photos were taken with an iPhone camera (Apple, Cupertino, CA) at the ocular of a modified stereo microscope, using light-emitting diode (LED) illumination in the other optical path of the microscope. (**A**) At pressures up to 335 GPa, hydrogen was transparent. The sample was both front and back illuminated in this and in (B); the less bright area around the sample is light reflected off of the Re gasket. (**B**) At this stage of compression, the sample was black and nontransmitting. The brighter area to the top right corner is due to the LED illumination, which was not focused on the sample for improved contrast. (**C**) Photo of metallic hydrogen at a pressure of 495 GPa. The sample is nontransmitting and observed in reflected light. The central region is clearly more reflective than the surrounding metallic Re gasket. The sample dimensions are ~8 to 10 μm, with thickness of ~1.2 μm (*26*).

At high pressure, the stressed culet of the diamond becomes absorptive, owing to closing down of the diamond band gap (5.5 eV at ambient) (*30*). This attenuated both the incident and reflected light and is strongest in the blue. Fortunately, this has been studied in detail by Vohra (*31*), who provided the optical density for both type I and II diamonds to very high pressures. We used this study (fig. S4) and determined the corrected reflectance (Fig. 3A). Last, after we measured the reflectance, we used very low laser power (642.6 nm laser wavelength) and measured the Raman shift of the diamond phonon to be 2034 cm^{-1}. This value fixes the end point of our rotation or load scale because the shift of the diamond phonon line has been calibrated. The linear 2006 scale of Akahama and Kawamura (*32*) gives a pressure of 495 ± 13 GPa when the sample was metallic. We do not include the potentially large systematic uncertainty in the pressure (*26*). This is the highest pressure point on our pressure versus load or rotation scale (fig. S3). Such curves eventually saturate; the pressure does not increase as the load is increased.

An analysis of the reflectance can yield important information concerning the fundamental properties of a metal. A very successful and easy-to-implement model is the Drude free-electron model of a metal (*33*). This model of a metal is likely a good approximation to relate reflectance to fundamental properties of a metal. A recent band structure analysis of the $I4_1/amd$ space group by Borinaga *et al.* (*9*) shows that for this structure, electrons in SMH are close to the free-electron limit, which supports the application of a Drude model. The Drude model has two parameters, the plasma frequency ω_p and the relaxation time τ. The plasma frequency is given by $\omega_p^2 = 4\pi n_e e^2/m_e$, where m_e and e are the electron mass and charge and n_e is the electron density. The complex index of refraction of MH is given by $N_H^2 = 1-\omega_p^2/(\omega^2 + j\omega/\tau)$, where ω is the angular frequency of the light. The MH is in contact with the stressed diamond that has an index of refraction N_D; this has a value of ~2.41 in the red region of the spectrum at ambient conditions. We measured reflectance $R(\omega) = |(N_D - N_H)/(N_D + N_H)|^2$ as a function of energy or (angular) frequency ω. We used a least-squares fit to the corrected reflectance data to determine the Drude parameters at 5 K, 32.5 ± 2.1 eV, and

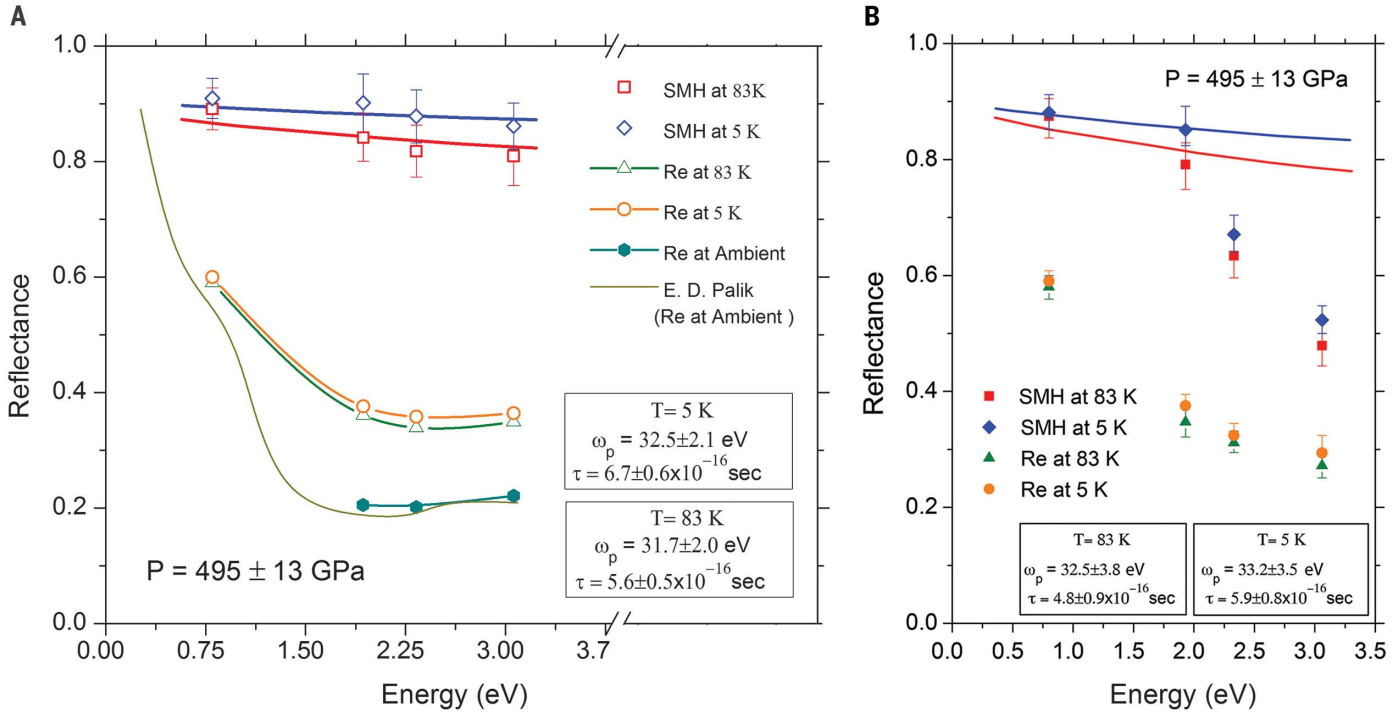

Fig. 3. Reflectance as a function of photon energy. (**A**) The energy dependence of the normal incidence reflectance off MH and the Re gasket, P = 495 GPa, at liquid-nitrogen and liquid-helium temperatures. We also show our measured reflectance from a surface of Re at a pressure of 1 bar at room temperature; this is in good agreement with literature values, verifying our measurement procedure. The reflectances have been corrected for absorption in the diamond. The lines through MH data are fits with a Drude free-electron model; the lines through the Re data points are guides to the eye. (**B**) A least-squares fit of the uncorrected reflectance to the two longest-wavelength data points for metallic hydrogen. The fit was carried out for reflectance at two temperatures, yielding the plasma frequencies and scattering times.

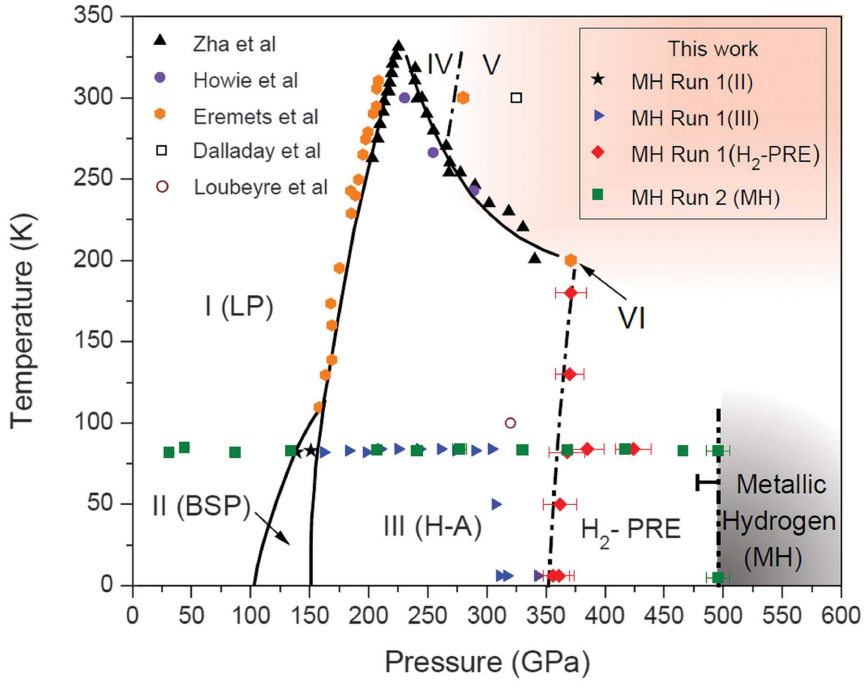

Fig. 4. The T-P phase diagram of hydrogen along pathway I of Fig. 1. The data show the thermodynamic pathway followed for our measurements. We also show other recent data for the phases at lower pressures from Zha *et al*. (*41*), Howie *et al*. (*23*), Eremets *et al*. (*25*), and Dias *et al*. (*24*). A transition claimed by Dalladay-Simpson *et al*. (*42*) at 325 GPa is plotted as a point, as is the earlier observation of black hydrogen by Loubeyre *et al*. (*28*).

$6.7 \pm 0.6 \times 10^{16}$ s. These values differ appreciably from a fit to the uncorrected data.

Because the diamond culet is stressed, we expect the index of refraction in the region of contact with the MH to change from the value at ambient pressure, and this might lead to an important uncertainty in the fitting parameters. The index of the diamond under pressure and uniaxial stress has been studied by Surh *et al*. (*34*). For hydrostatic pressures up to 450 GPa, the pressure dependence is rather weak; however, for uniaxial stressed diamond the change of index can be substantial. We fitted data for values of 2.12 for extreme uniaxial stress along the [001] crystal direction and 2.45 along the [100] and [010] directions, corresponding to a sample pressure of 250 GPa (*34*). This resulted in an uncertainty in the Drude parameters that was much smaller than that because of the uncertainty in the measured reflectance (Fig. 3). We fit the reflectance using a value N_D = 2.41, yielding the values for the Drude parameters shown in Fig. 3 and Table 1.

The pressure-temperature phase diagram of hydrogen along pathway I is shown in Fig. 4, focusing on the lower-temperature region. With increasing pressure, hydrogen enters the phase H_2-PRE at 355 GPa, and this is followed by the phase line based on the two points at temperature (T) = 83 and 5.5 K for the transition to MH. (*24*). Because we changed the pressure in larger

Table 1. Elements of the first column of the periodic table. We compare the electron density (calculated from the plasma frequency) in the second column with the atom density in the third column and see that there is about 1 electron per atom. The plasma frequencies are from (*43*). The data are for hydrogen at 5.5 K; all other elements are at 77 K. A definition of r_s/a_0 is provided in (*26*).

Element	$n_e = \frac{m_e \omega_p^2}{4\pi e^2}$ (10^{22}/cm^3)	n_a (10^{22}/cm^3)	r_s/a_o	Plasma frequency (eV)
Hydrogen	81 ± 17	66.5 to 86.0	1.255 to 1.34	33.2 ± 3.5
Lithium	3.68	4.63	3.25	7.12
Sodium	2.36	2.54	3.93	5.71
Potassium	1.00	1.33	4.86	3.72

increments by rotating a screw, there could be a systematic uncertainty of ~25 GPa on the low-pressure side of the phase line. The transition to MH may have taken place while increasing the pressure from ~465 to 495 GPa (*26*). We believe that the metallic phase is most likely solid, based on recent theory (*35*), but we do not have experimental evidence to discriminate between the solid and liquid states. We detected no visual change in the sample when the temperature was varied between 83 and 5.5 K. A theoretical analysis predicted a maximum in the pressure-temperature melting line of hydrogen (*36*). The maximum was first experimentally observed by Deemyad and Silvera (*37*). One speculation has the melting line (Fig. 1) extrapolating to the $T = 0$ K limit at high pressure, resulting in liquid MH in this limit (*10*, *36*). An extrapolation of the negative P,T slope was supported by a calculation (*38*) showing that the liquid atomic phase might be the ground state in the low-temperature limit. On the other hand, Zha (*39*) has extended the melting line to 300 GPa and finds a slope that is shallower than the extrapolation shown in Fig. 1. The vibron spectra at low temperature in phase H_2-PRE correspond to spectra from a solid. Although H_2-PRE is solid, the possibility remains that an increase in translational zero-point energy occurs when molecular hydrogen dissociates, resulting in a liquid ground state.

The plasma frequency $\omega_p = 32.5 \pm 2.1$ eV is related to the electron density and yields a value of $n_e = 7.7 \pm 1.1 \times 10^{23}$ particles/cm^3. No experimental measurements exist for the atom density at 500 GPa. Theoretical estimates range from ~6.6 to 8.8 × 10^{23} particles/cm^3 (*26*). This is consistent with one electron per atom, so molecular hydrogen is dissociated, and the sample is atomic MH, or the WH phase. Whereas some predictions suggest metallization of molecular hydrogen at high pressure (*3*), this requires one electron for every two atoms instead. MH at 495 GPa is about 15-fold denser than zero-pressure molecular hydrogen. We compared MH with other elements in the first column of the periodic table (Table 1), which has a remarkable contrast in properties.

We have produced atomic MH in the laboratory at high pressure and low temperature. MH may have an important impact on physics and perhaps will ultimately find wide technological application. Theoretical work suggests a wide array of interesting properties for MH, including high-temperature superconductivity and superfluidity (if a liquid) (*40*). A looming challenge is to quench MH and if so, study its temperature stability to see whether there is a pathway for production in large quantities.

REFERENCES AND NOTES

1. V. L. Ginzburg, *Rev. Mod. Phys.* **76**, 981–998 (2004).
2. E. Wigner, H. B. Huntington, *J. Chem. Phys.* **3**, 764–770 (1935).
3. J. M. McMahon, M. A. Morales, C. Pierleoni, D. M. Ceperley, *Rev. Mod. Phys.* **84**, 1607–1653 (2012).
4. J. McMinis, R. C. Clay, D. Lee, M. A. Morales, *Phys. Rev. Lett.* **114**, 105305 (2015).
5. S. Azadi, B. Monserrat, W. M. C. Foulkes, R. J. Needs, *Phys. Rev. Lett.* **112**, 165501 (2014).
6. J. M. McMahon, D. M. Ceperley, *Phys. Rev. Lett.* **106**, 165302–165304 (2011).
7. N. W. Ashcroft, *Phys. Rev. Lett.* **21**, 1748–1749 (1968).
8. J. M. McMahon, D. M. Ceperley, *Phys. Rev. B* **84**, 144515 (2011).
9. M. Borinaga, I. Errea, M. Calandra, F. Mauri, A. Bergara, *Phys. Rev. B* **93**, 174308 (2016).
10. E. G. Brovman, Y. Kagan, A. Kholas, *Sov. Phys. JETP* **34**, 1300–1315 (1972).
11. J. Cole, I. F. Silvera, J. P. Foote, Conceptual launch vehicles using metallic hydrogen propellant. *AIP Conf. Proc. 978*, M. S. El-Genk, Ed. (STAIF-2008, 2008), pp. 977–984.
12. M. Zaghoo, A. Salamat, I. F. Silvera, *Phys. Rev. B* **93**, 155128 (2016).
13. S. T. Weir, A. C. Mitchell, W. J. Nellis, *Phys. Rev. Lett.* **76**, 1860–1863 (1996).
14. V. E. Fortov *et al.*, *Phys. Rev. Lett.* **99**, 185001–185004 (2007).
15. M. D. Knudson *et al.*, *Science* **348**, 1455–1460 (2015).
16. C. Pierleoni, M. A. Morales, G. Rillo, M. Holzmann, D. M. Ceperley, *Proc. Natl. Acad. Sci. U.S.A.* **113**, 4953–4957 (2016).
17. G. E. Norman, I. M. Saitov, V. V. Stegailov, *Plasma Phys.* **55**, 215–221 (2015).
18. I. F. Silvera, *Rev. Mod. Phys.* **52**, 393–452 (1980).
19. I. F. Silvera, R. J. Wijngaarden, *Phys. Rev. Lett.* **47**, 39–42 (1981).
20. R. J. Hemley, H. K. Mao, *Phys. Rev. Lett.* **61**, 857–860 (1988).
21. H. E. Lorenzana, I. F. Silvera, K. A. Goettel, *Phys. Rev. Lett.* **63**, 2080–2083 (1989).
22. M. I. Eremets, I. A. Troyan, *Nat. Mater.* **10**, 927–931 (2011).
23. R. T. Howie, C. L. Guillaume, T. Scheler, A. F. Goncharov, E. Gregoryanz, *Phys. Rev. Lett.* **108**, 125501 (2012).
24. R. Dias, O. Noked, I. F. Silvera, New low temperature phase transition in dense hydrogen: The phase diagram to 421 GPa; arXiv:1603.02162v1 (2016).
25. M. I. Eremets, I. A. Troyan, A. P. Drozdov, Low temperature phase diagram of hydrogen at pressures up to 380 GPa. A possible metallic phase at 360 GPa and 200 K; https://arxiv.org/abs/1601.04479 (2016).
26. Materials and methods are available as supplementary materials.
27. M. I. Eremets, *J. Raman Spectrosc.* **34**, 515–518 (2003).
28. P. Loubeyre, F. Occelli, R. LeToullec, *Nature* **416**, 613–617 (2002).
29. E. D. Palik, Ed., *Handbook of Optical Constants of Solids* (Elsevier, 1997), vol. III.
30. A. L. Ruoff, H. Luo, Y. K. Vohra, *J. Appl. Phys.* **69**, 6413–6416 (1991).
31. Y. K. Vohra, in *Proceedings of the XIII AIRAPT International Conference on High Pressure Science and Technology* (World Scientific, 1991).
32. Y. Akahama, H. Kawamura, *J. Appl. Phys.* **100**, 043516 (2006).
33. F. Wooten, *Optical Properties of Solids* (Academic Press, 1972).
34. M. P. Surh, S. G. Louie, M. L. Cohen, *Phys. Rev. B Condens. Matter* **45**, 8239–8247 (1992).
35. J. Chen *et al.*, *Nat. Commun.* **4**, 2064 (2013).
36. S. A. Bonev, E. Schwegler, T. Ogitsu, G. Galli, *Nature* **431**, 669–672 (2004).
37. S. Deemyad, I. F. Silvera, *Phys. Rev. Lett.* **100**, 155701 (2008).
38. C. Attaccalite, S. Sorella, *Phys. Rev. Lett.* **100**, 114501 (2008).
39. C. S. Zha, "Hot-dense hydrogen study up to 300 GPa," presented at APS March Meeting 2016, Baltimore, MD, 17 March 2016; http://meetings.aps.org/link/BAPS.2016.MAR.V21.3.
40. E. Babaev, A. Sudbø, N. W. Ashcroft, *Nature* **431**, 666–668 (2004).
41. C.-S. Zha, Z. Liu, R. J. Hemley, *Phys. Rev. Lett.* **108**, 146402–146407 (2012).
42. P. Dalladay-Simpson, R. T. Howie, E. Gregoryanz, *Nature* **529**, 63–67 (2016).
43. C. Kittel, *Introduction to Solid State Physics* (John Wiley & Sons, ed. 7, 1996).

ACKNOWLEDGMENTS

We thank O. Noked, M. Zaghoo, R. Husband, and C. Meyers for assistance and discussions. O. Noked provided valuable assistance developing our general optical setup; R. Husband did the reactive ion etching, as well as the alumina coating of the diamonds; and M. Turner of the Walsworth group provided help for annealing our diamonds. The NSF, grant DMR-1308641, and the U.S. Department of Energy Stockpile Stewardship Academic Alliance Program, grant DE-NA0003346, supported this research. Partial support was provided by a grant from A. Silvera and K. Silvera. Preparation of diamond surfaces was performed in part at the Center for Nanoscale Systems (CNS), a member of the National Nanotechnology Infrastructure Network (NNIN), which is supported by NSF under NSF award ECS-0335765. CNS is part of Harvard University. The data reported in this paper are tabulated and available from the authors. Both authors contributed equally to all aspects of this research.

SUPPLEMENTARY MATERIALS

www.sciencemag.org/content/355/6326/715/suppl/DC1
Materials and Methods
Figs. S1 to S8
Databases S1 to S14
References (*44*–*60*)

5 October 2016; accepted 13 January 2017
Published online 26 January 2017
10.1126/science.aal1579